



Synthesis, Characterization, Optical, Electrochemical and Current-Voltage Characteristics of Coumarin Dyes

K. V. Basavarajappa^{1,2} · Y. Arthoba Nayaka¹ · R. O. Yathisha¹ · P. Manjunatha¹

Received: 20 June 2019 / Accepted: 3 September 2019
© Springer Science+Business Media, LLC, part of Springer Nature 2019

Abstract

A series of coumarin dyes having common acceptor and pi spacer with different donors were synthesized and characterized by spectroscopic techniques. The TiO₂ nanoparticle has been synthesized by sol-gel method and characterized by X-ray diffraction, scanning electron microscopy and energy dispersive spectroscopy. Photophysical and electrochemical properties have been investigated. The band gap, molar absorption coefficient and energies of frontier molecular orbitals (FMO) have been calculated. The results showed that an electron releasing group helps in tuning the band gap. The geometry optimization and energies of FMO were obtained by density functional theory calculations. The calculated global chemical parameters help in understanding the intrinsic donor-acceptor properties of the synthesized dye molecules. The result of current-voltage characteristics showed good photocurrent response under illumination condition.

Keywords Coumarin · Band gap · I-V characteristics · TiO₂

Introduction

Energy is a vital component to our life and the use of energy is increasing with human advancement and industrial development [1]. Most of the present-day energy sources are from non-renewable energy forms like fossil fuels, thermal energy, etc. and these sources are going to decline day by day. To overcome this situation there is a great need for cheaper and cleaner energy sources. Solar energy is abundant and readily available, so, one should make solar energy a priority for our future energy. The development of dye-sensitized solar cells (DSSCs), the third generation of photovoltaics using small

organic molecules helps us to meet the urgent needs for cheaper and cleaner energy. The dye-sensitized TiO₂ solar cells have the advantages of low-cost, eco-friendly, better conversion efficiency and so on [2].

Small organic molecules have been attracting great attention in the past few years due to their unique properties of the low-cost, easy synthetic procedure, flexibility in designing organic photovoltaics. Among the small organic molecules, coumarin dyes have been recognized as one of the good organic dye photosensitizers [3]. Therefore, it was planned to synthesize the coumarin molecules containing different electron-donating groups and electron-withdrawing nitro group. The chemical structures of the synthesized molecules and the numbering of simple coumarin skeleton are as shown in Fig. 1.

The above molecules were prepared by a facile novel method. This novel procedure is found to be a more useful and convenient method for the preparation of 2,4-dinitrophenylhydrazones of coumarin than the reported methods cited elsewhere [4–7]. The proposed method is fast, simple, avoids the use of corrosive chemicals and there is no need of column chromatographic separation of the products. The detailed synthetic procedure is given in the [Experimental Section](#).

Out of many semiconducting metal oxides, TiO₂ nanoparticle appears to be more versatile because due to its very high

Electronic supplementary material The online version of this article (<https://doi.org/10.1007/s10895-019-02436-7>) contains supplementary material, which is available to authorized users.

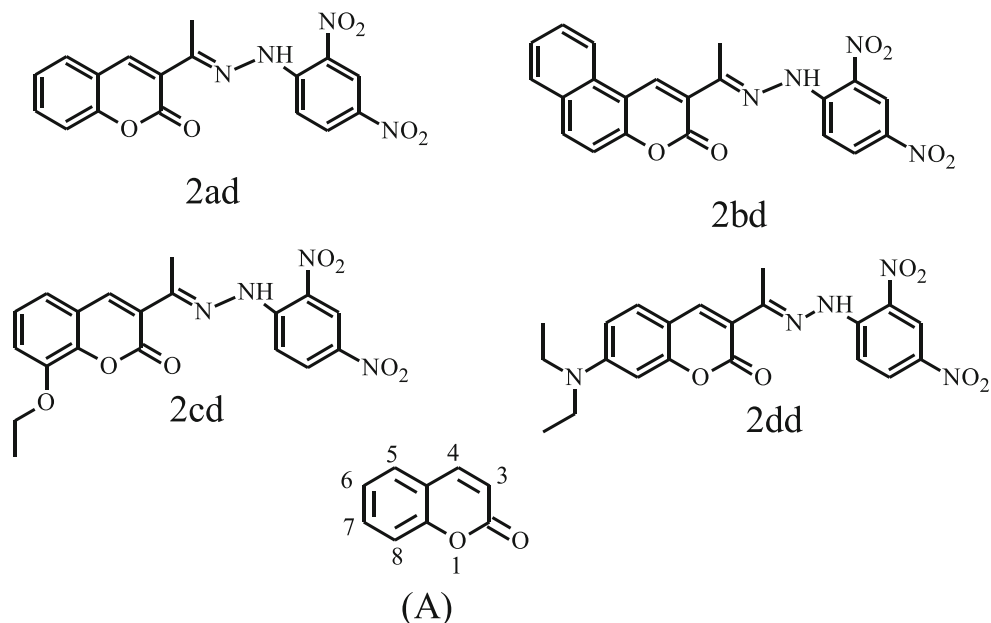
✉ Y. Arthoba Nayaka
drarthoba@yahoo.co.in; basu.kv2019@gmail.com

K. V. Basavarajappa
basu.kv@gmail.com

¹ Department of PG Studies and Research in Chemistry, Kuvempu University, Jnanasahyadri, Shankaraghatta, Karnataka 577451, India

² Department of Chemistry, Government First Grade College, Davanagere, Karnataka 577004, India

Fig. 1 The chemical structures of coumarin molecules (2ad-2dd) and numbering of simple coumarin (A)



roughness factor and it provides extremely favorable and efficiently irreversible entropic and enthalpic driving forces for charge injection. Low recombination within the semiconductor matrix as well as between the semiconductor and the hole-transporting layer (HTL) allows for very efficient electron transport to the anode. Light scattering within the porous crystalline structure increases the radiation path-length and thus improves photon harvesting [8].

In this work, the target coumarin molecules were synthesized by facile novel procedure and characterized using analytical methods. The TiO₂ nanoparticles were synthesized by a modified literature procedure using a sol-gel method. Absorption properties of dyes in solution and dyes coated on TiO₂ nanoparticle were tested. The energies of HOMO and LUMO of the dyes were determined by cyclic voltammetric studies and compared with theoretical values obtained by DFT calculations. The current-voltage (I-V) characteristics were performed by dyes coated TiO₂ nanoparticles. The results obtained were discussed and concluded.

Experimental Section

Materials and Instruments

The analytical grade 2-hydroxybenzaldehyde, ethylacetoacetate (EAA), piperidine, N, N-dimethylformamide (DMF), 1,4-dioxane, ethyl alcohol, 2-propanol and glacial acetic acid were purchased from SD Fine-Chem Limited. 2,4-dinitrophenylhydrazine (2,4-DNP) (Extra pure) was purchased from HiMedia Laboratories Pvt. Ltd.. Titanium tetrachloride (TiCl₄) was obtained from Avra

synthesis private limited. 2-hydroxy-1-naphthaldehyde, 4-(diethylamino) salicylaldehyde, 3-ethoxysalicylaldehyde (technical grade) and tetrabutylammonium hexafluorophosphate (electrochemical grade) were purchased from Sigma-Aldrich. All the chemicals were used for the experiments as such without further purification. Oven-dried glasswares were used to carry out the reactions. The reactions were monitored by thin-layer chromatography (TLC) using silica gel 60 F₂₅₄ (Merck) and a mixture of ethyl acetate (EA) and n-hexane (60–80 °C boiling mixtures) as mobile phase. The TLC spots were visualized under UV light. Melting points were determined using open-ended capillary tubes and were uncorrected. FTIR spectra were recorded on KBr pellets using Bruker Alpha-T spectrophotometer. ¹H NMR spectra were recorded on a VNMRS-400 Agilent-NMR spectrometer using Tetramethylsilane (TMS) as an internal standard. Chemical shift (δ) values were expressed in parts per million (ppm) units. Mass Spectra (MS) were recorded using Water's SYNAPT G2 QTOF LCMS instrument. UV absorption spectra were recorded using UV-Visible-NIR spectrometer [USB 4000, Ocean Optics, USA] in anhydrous solvents. The electrochemical measurements obtained by CHI660D electrochemical workstation using the three-electrode system. The crystalline structure of TiO₂ was obtained by X-ray diffractometer (XRD) (Rigaku), and the surface morphology and crystalline structure were obtained by scanning electron microscopy (SEM) (ZEISS EVO LS15). The elemental analysis of TiO₂ nanoparticle was conducted by energy dispersive analyzer using X-rays (EDAX) (Thermo Scientific Noran 7) and I-V characterization was performed by Keithley source meter with USB GRIB adaptor [Model: 2401].

Synthesis

General Procedure for the Solvent Free Synthesis of 3-Acetyl Coumarin Derivatives (2a-2d)

The solvent-free method was selected for the synthesis of 3-acetyl coumarins via Knoevenagel condensation [9]. This method involves simple operation, waste minimization and easier product work-up. The synthetic procedure involves an equivalent mixture of derivatives of salicylaldehyde (1a-1d, 10.0 mmol), ethyl acetoacetate (10.0 mmol) and a few drops of piperidine were mixed and ground well for 5 min at room temperature (rt). The reaction mixtures were neutralized with HCl (4 N) and then, the so obtained substituted 3-acetyl coumarins (2a-2d) were isolated by filtration. The IR, ¹H NMR and Mass spectral analysis was used for structural confirmation of the synthesized molecules. The synthetic pathway is as shown in Scheme 1. IR, ¹H NMR and Mass spectra of the samples are shown in supplementary material S1, S2 and S3 respectively.

3-Acetyl-2H-Chromen-2-One (2a)

Recrystallization: ethanol; color and appearance: colorless needle-shaped crystals. Yield: 77% and mp 120–124 °C. IR (KBr, v, cm⁻¹): 1726 (lactone C=O), 1682 (CH₃-C=O), 3080 and 3052 (Ar C-H), 2925.81 (CH₃ C-H). ¹H NMR (400 MHz, CDCl₃) δ (ppm): 2.633 (3H, s, COCH₃), 7.375–8.637 (5H, m, ArH). MS-AP⁺ (m/z) found: 189.0318 (M + H)⁺; calculated for C₁₁H₈O₃: 188.0468 (M⁺).

2-Acetyl-3H-Benzof[*f*]Chromen-3-One (2b)

Recrystallization: ethanol; color and appearance: bright yellow crystals. Yield: 67% and mp 174–176 °C. IR (KBr, v, cm⁻¹): 1737 (lactone C=O), 1673 (CH₃-C=O), 3058 and 3017 (Ar C-H), 2930.06 (CH₃ C-H). ¹H NMR (400 MHz, CDCl₃) δ (ppm): 2.633 (3H, s, COCH₃), 7.598–9.271 (7H, m, ArH). MS-AP⁺ (m/z) found: 239.0558 (M + H)⁺; calculated for C₁₅H₁₀O₃: 238.0624 (M⁺).

3-Acetyl-8-Ethoxy-2H-Chromen-2-One (2c)

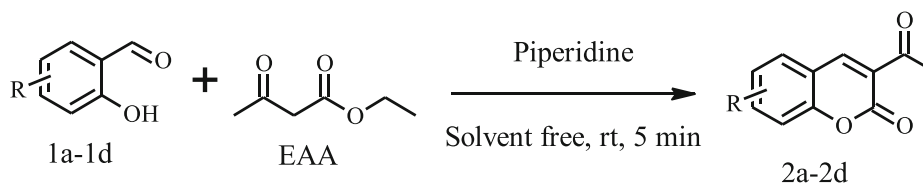
Recrystallization: ethanol; color and appearance: yellow powder. Yield: 86% and mp 122–124 °C. IR (KBr, v, cm⁻¹): 1722 (lactone C=O), 1677 (CH₃-C=O), 3095 and 3349 (Ar C-H), 2930 (CH₃ C-H). ¹H NMR (400 MHz, CDCl₃) δ (ppm): 1.484–1.519 (3H, t, CH₂CH₃), 2.713 (3H, s, COCH₃), 4.161–4.214 (2H, q, OCH₂) 7.418–98.455 (4H, m, ArH). MS-AP⁺ (m/z) found: 233.0692 (M + H)⁺; calculated for C₁₃H₁₂O₄: 232.0730 (M⁺).

3-Acetyl-7-(Diethylamino)-2H-Chromen-2-One (2d)

Recrystallization: ethanol; color and appearance: yellow crystals. Yield: 77% and mp 146–148 °C. IR (KBr, v, cm⁻¹): 1720 (lactone C=O), 1662 (CH₃-C=O), 3118 and 2964 (Ar C-H), 2925 (CH₃ C-H). ¹H NMR (400 MHz, CDCl₃) δ (ppm): 1.200–1.235 (6H, t, CH₃CH₂), 2.652 (3H, s, CH₃CO) 3.406–3.460 (4H, CH₂CH₃), 6.437–8.405 (4H, m, ArH). MS-AP⁺ (m/z) found: 260.1194 (M + H)⁺; calculated for C₁₅H₁₇NO₃: 259.1203 (M⁺).

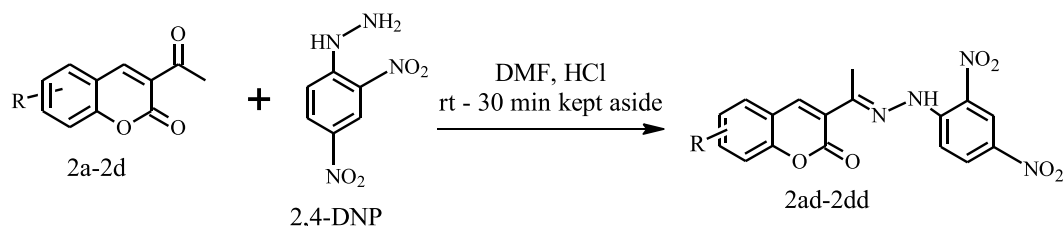
General Procedure for the Synthesis of 2,4-Dinitrophenylhydrazones of 3-Acetyl Coumarins (2ad-2dd)

3-acetyl coumarins (2a-2d) (2.23 mmole) were added to a solution of 2,4-dinitrophenylhydrazine (2.52 mmole) in dimethylformamide (5 mL) in a 50 mL beaker and the mixture was swirled to get a homogenous solution, added two drops of HCl (35%) and kept for 30 min at room temperature. The obtained solid product was filtered and washed with 20 mL of 2 N aqueous hydrochloric acid, 30 mL of water and 30 mL of cold 95% aqueous ethanol. The crude product was dried and recrystallized from 1,4-dioxane to get pure hydrazones (41–68%) as orange-yellow powder. The structures of newly synthesized compounds are in agreement with their IR, ¹H NMR and Mass spectral data and are shown in S4, S5 and S6 (supporting information). The synthetic pathway is as shown in Scheme 2.



Where, R=H: 1a and 2a, R= 5, 6-benzo: 1b and 2b, R= OCH₃: 1c and 2c and R=N(Et)₂: 1d and 2d.

Scheme 1 Synthesis of 3-acetyl coumarins (2a-2d)



Where, R=H: 2a and 2ad, R= 5, 6-benzo: 2b and 2bd, R= OCH₃: 2c and 2cd and R=N(Et)₂: 2d and 2dd

Scheme 2 Synthesis of 2,4-dinitrophenylhydrazones of 3-acetyl coumarins (2ad-2dd)

3-[(1E)-1-[2-(2, 4-Dinitrophenyl)Hydrazinylidene] Ethyl]-2H-Chromen-2-One (2ad)

Recrystallization: 1,4-dioxane; color and appearance: orange crystal. Isolated yield: 56% and mp 258–260 °C. IR (KBr, ν , cm^{-1}): 3316 (N-H), 3114 (Ar C-H), 2922 (CH₃ C-H), 1723 (lactones C=O), 1610 (-C=N-), 1507 and 1328 (asy and sy stretch of NO₂). ¹H NMR (400 MHz, CDCl₃) δ (ppm): 2.492 (3H, COCH₃), 7.247–9.176 (8H, m, ArH) and 11.383 (1H, s, NH). MS-AP⁺ (m/z) found: 367.0741 (M-H)⁺; calculated for C₁₇H₁₂N₄O₆: 368.0751 (M⁺).

2-[(1E)-1-[2-(2,4-Dinitrophenyl)Hydrazinylidene] Ethyl]-3H-Benzo[f]Chromen-3-One (2bd)

Recrystallization: 1,4-dioxane; color and appearance: orange-red crystals. Isolated yield: 41% and mp 240–244 °C. IR (KBr, ν , cm^{-1}): 3308 (N-H), (3113 and 3072 (Ar C-H), 2921 (CH₃ C-H), 1618 (-C=N-), 1723 (lactone C=O), 1510 and 1307 (asy and sy str of NO₂). ¹H NMR (400 MHz, CDCl₃) δ (ppm): 2.569 (3H, s, COCH₃), 7.510–9.200 (10H, m, ArH) and 11.459 (1H s, NH). MS-AP⁺ (m/z) found: 418.9489 (M + H)⁺; calculated for C₂₁H₁₄N₄O₆: 418.0908 (M⁺).

3-[(1E)-1-[2-(2,4-Dinitrophenyl)Hydrazinylidene] Ethyl]-8-Ethoxy-2H-Chromen-2-One (2cd)

Recrystallization: 1,4-dioxane; color and appearance: orange crystals. Isolated yield: 50% and mp 250–252 °C. IR (KBr, ν , cm^{-1}): 3449 (N-H), 3113 and 3072 (Ar C-H), 2921 (CH₃ C-H), 1723 (lactone C=O), 1613 (-C=N-), 1510 and 1333 (asy and sy str of NO₂). ¹H NMR (400 MHz, CDCl₃) δ (ppm): 1.506–1.541 (3H, t, OCH₂CH₃), 2.489 (3H, s, COCH₃), 4.185–4.237 (2H, q, OCH₂), 7.123–9.177 (7H, m, ArH) and 11.380 (1H, s, NH). MS-AP⁺ (m/z) found: 413.9733 (M + H)⁺; calculated for C₁₉H₁₆N₄O₇: 413.1092 (M + H)⁺.

7-(Diethylamino)-3-[(1E)-1-[2-(2,4-Dinitrophenyl)Hydrazinylidene]Ethyl]-2H-Chromen-2-One (2dd)

Recrystallization: 1,4-dioxane; color and appearance: red shiny crystals. Isolated yield: 68.4% and mp 262–264 °C. IR

(KBr, ν , cm^{-1}): 3288 (N-H), 3113 and 3072 (Ar C-H), 2921 (CH₃ C-H), 1723 (lactone C=O), 1615 (-C=N-), 1512 and 1335 (asy and sy stretch of NO₂). ¹H NMR (400 MHz, CDCl₃) δ (ppm): 1.219–1.255 (6H, t, CH₃), 2.488 (3H, s, COCH₃), 3.422–3.475 (4H, q, NCH₂), 6.498–9.155 (7H, m, ArH) and 11.358 (1H, s, NH). MS-AP⁺ (m/z) found: 440.9984 (M + H)⁺; calculated for C₂₁H₂₁N₅O₆:440.1565 (M + H)⁺.

Synthesis of TiO₂ Nanoparticles

The sol-gel method has been used to synthesize the TiO₂ nanoparticles using modified reported procedure [10]. A 4 ml of analytical grade TiCl₄ was added dropwise to 1:1 solution of 2-propanol and glacial acetic acid under vigorous stirring at room temperature. The resultant solution was stirred overnight and then dried in a hot air oven for about 6 h. Later the precipitate formed was calcined at 500 °C for about 2 h soaking time.

Dye Coating

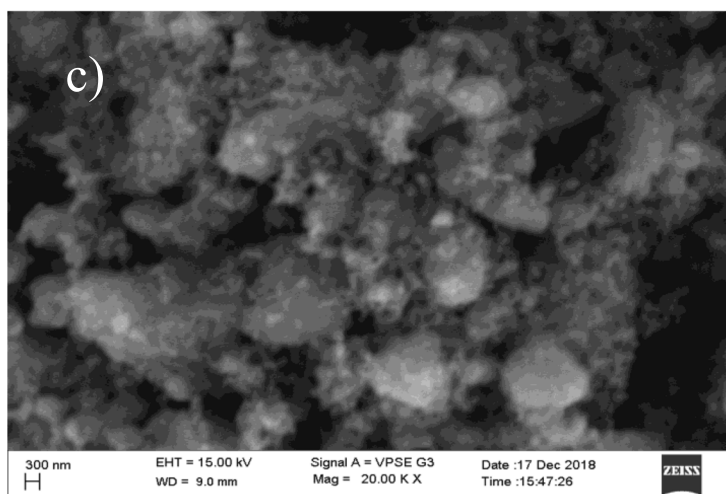
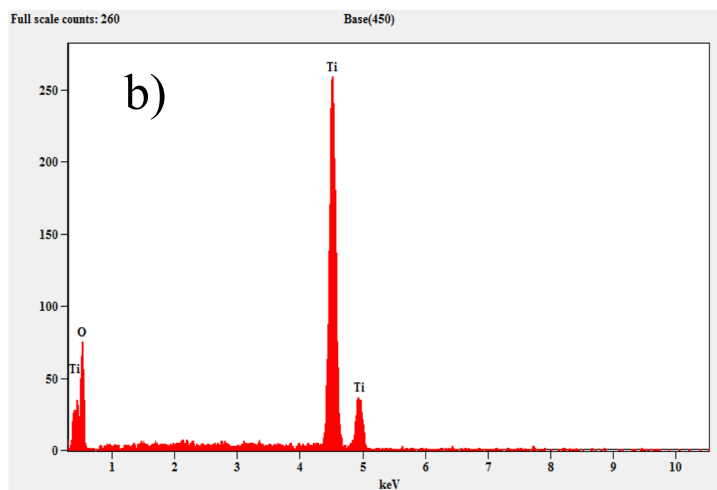
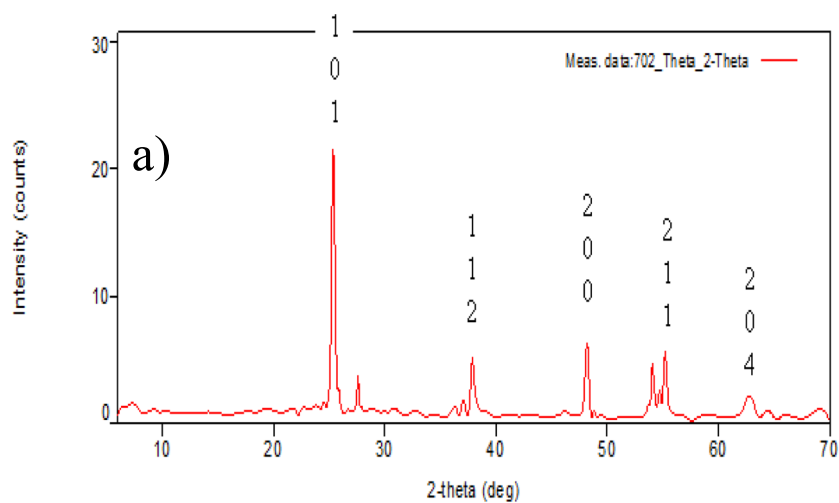
Synthesized TiO₂ nanoparticles were ground well to make a uniform sample of fine nanoparticles. These nanoparticles were mixed with a chloroform solution of coumarin dyes (3.5 mM, 2ad-2dd) to prepare a slurry. A thin layer of this slurry was uniformly deposited on the surface of well-cleaned glass plates by dip coat method. Dye coated glass plates were kept aside for 30 min at room temperature for solvent evaporation, later in a hot air oven for 7 h at 70 °C. After that, it was cooled down to rt. and taken out for absorption and I-V studies. The electrical connection was made by inserting the copper wire.

Result and Discussion

Spectral Characterization

The target compounds (2ad-2dd) were synthesized by a novel approach, which involves the condensation of 3-acetyl coumarins (2a-2d) with 2,4-DNP in DMF as depicted in Scheme 2. The IR, ¹H NMR and MS techniques were used for

Fig. 2 **a** XRD-Pattern of TiO₂, **b** EDAX Spectrum of TiO₂ and **c** SEM-Image of TiO₂



structural elucidation of the synthesized dyes. The strong IR absorption band appeared around 1713–1730 cm⁻¹

(supporting information S4) corresponds to lactone of coumarin skeleton. The absence of peaks around 1662–1682 cm⁻¹ in

Table 1 Optical and structural properties of TiO₂

Entry	λ_{\max} (nm)	λ_{edge} (nm)	E_g^{opt} (eV)	Average crystalline size(D) nm
TiO ₂	354.24	448.65	2.76 ^a	30.5

^a. $E_g^{\text{opt}} = 1240/\lambda_{\text{edge}}$ eV, [11]

the products 2ad-2dd clearly indicated the conversion of the ketonic carbonyl group of the starting materials 2a-2d (supporting information S1) to the imine group. The new band appeared around 1610–1618 cm⁻¹ further confirms the imine (C=N) functional group. Moreover, stretching frequencies appeared around 1507–1512 cm⁻¹ and 1328–1335 cm⁻¹ are responsible for the asymmetric and symmetric stretch of Ar-NO₂ group. The proton of N-H for all the molecules appeared around $\delta \sim 11$ as a singlet peak (supporting information S5). From the mass spectrometry, the calculated molecular weights of the synthesized compounds were in good agreement with the experimentally obtained values (supporting information S6).

XRD, EDAX and SEM Analysis

Figure 2a shows the powder X-ray diffraction patterns of synthesized TiO₂ nanoparticles. The Figure indicates phase purity and structural parameters of TiO₂. The X-ray diffraction patterns show one intense peak at (101) plane, three moderately intense peaks corresponds to (112), (200), and (211) planes and less intense peak at (204) plane. It suggested that the synthesized nanomaterial has a tetragonal system with anatase structure, which is further confirmed from the JCPDS No.84–1285 ($a = 3.784$ and $c = 9.512$). The chemical elements detection with their relative abundance can be obtained from EDAX analysis and is as shown in Fig. 2b, it confirms the purity of the synthesized nanoparticle TiO₂. Figure 2c, scanning electron micrograph reveals the surface morphology of

synthesized TiO₂ nanoparticles. The optical band gap was calculated and tabulated in Table 1. Debye-Scherrer Eq. (1) is used to calculate the average crystalline size (D) [12].

$$D = 0.9\lambda/\beta \cos\theta \quad (1)$$

Where, β is the full width at half maxima in radians, λ is the wavelength of CuK α X-ray radiation used ($\lambda = 0.154$ nm) and θ is the Bragg's reflection angle in degrees. The calculated data of optical and structural parameters of TiO₂ are given in Table 1.

Photophysical Properties

The absorption spectra of coumarin dyes in DMF (1×10^{-5} M) and the dyes coated on TiO₂ nanoparticles are shown in Fig. 3a and b. The optical band gap (E_g^{opt}) and molar absorption coefficient (ϵ) are calculated and tabulated in Table 2 [13]. From the Table, it is cleared that the wavelength maximum of dyes in DMF has been shifted to higher wavelength for 2dd compared to other coumarin dyes. This bathochromic shift of 2dd is ascribed to the effect of strong electron releasing diethylamine group and hence decreasing the band gap. The synthesized compounds have higher molar absorption coefficient (ϵ) values than that of typical C343 and NKX series of dyes [14]. The dyes coated TiO₂ nanoparticles show broadening of absorption maxima in comparison to coumarin dyes in DMF solution. This broadening clearly shows that there is a good electron communication between dye and TiO₂. In addition, broadening

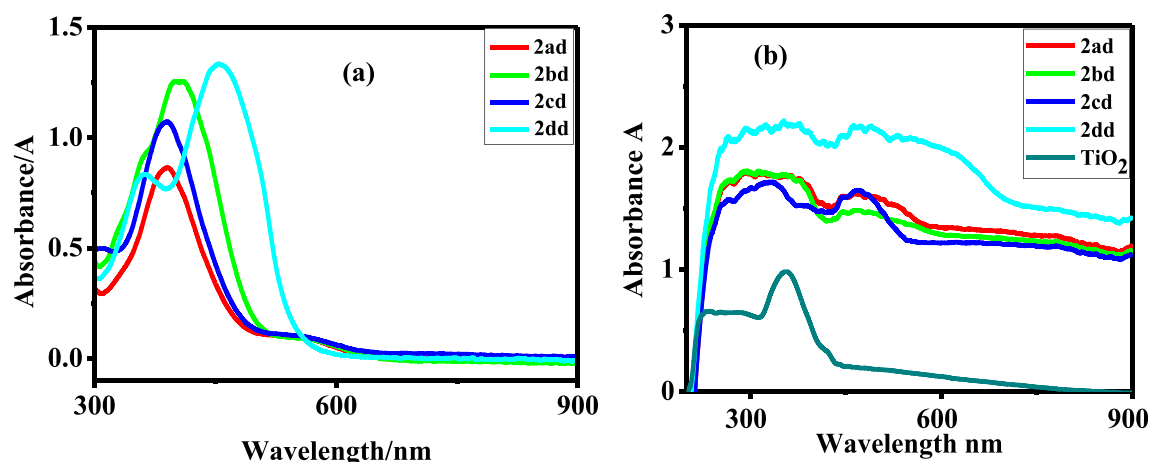


Fig. 3 Absorption spectra of coumarin derivatives. **a** In DMF and **b** On TiO₂

Table 2 Absorption properties of coumarin derivatives

Entry	λ_{\max} (nm)	λ_{edge} (nm)	$E_{\text{g}}^{\text{opt}}$ (eV) ^a	Molar absorption coefficient (ϵ) $10^5 \text{ M}^{-1} \text{ cm}^{-1}$
2ad	390.15	479.44	2.59	0.87
2bd	406.82	498.19	2.49	1.26
2cd	389.75	491.78	2.52	1.08
2dd	453.34	549.64	2.26	1.34

$$^a E_{\text{g}}^{\text{opt}} \text{ (eV)} = 1240/\lambda_{\text{edge}}(\text{nm})$$

of the absorption spectrum is advantageous for better harvesting of solar energy and hence to get a large photocurrent [11].

Electrochemical Studies

Electrochemical properties of synthesized dyes were determined by cyclic voltammetric studies in DMF using pencil graphite as the working electrode, Ag/Ag⁺ as the reference electrode, platinum as counter electrode and 0.2 M tetrabutylammonium hexafluorophosphate as supporting electrolyte. The oxidation onset potentials of dyes were found to be 0.3727 V, 0.2873 V, 0.3915 V and 0.1788 V for 2ad, 2bd, 2cd and 2dd respectively. The energies of highest occupied molecular orbital (HOMO) and lowest unoccupied molecular orbital (LUMO) were calculated using the formula: $E_{\text{HOMO}} = -(E_{\text{onsetox}} + 5.1)$ eV and $E_{\text{LUMO}} = E_{\text{HOMO}} + E_{\text{g}}^{\text{opt}}$, where, E_{onsetox} is the onset oxidation potential in V, $E_{\text{g}}^{\text{opt}}$ is the optical band gap in eV, and 5.1 eV is the assuming electrochemical potential of ferrocene/ferrocenium (Fc/Fc⁺) vs. vacuum [15]. The obtained values are summarized in Table 3. The cyclic voltammograms of the compounds 2ad-2dd are as shown in Fig. 4. Table 3 reveals that HOMO energy levels are increasing in the following order -5.4915 (2cd), -5.4723 (2ad), -5.387 (2bd), and -5.2788 eV (2dd). DFT calculated HOMO values were also follows the same trend (Table 3).

The observed oxidation peaks in Fig. 4 at A, B, C and D are respectively due to the electron transfer from HOMO of 2ad, 2bd, 2cd and 2dd to the electrode. The least negative value of 2dd is due to the presence of strong electron-donating group

diethylamine and the less negative value in case of 2bd is due to the extended conjugation of coumarin backbone, and hence the electron releasing groups/extended conjugation destabilizes the HOMO level [13].

From the theory of DSSC for the effective injection of electrons into the conduction band (CB) of TiO₂, the LUMO levels of the dye must be sufficiently higher energy than the conduction band energy of semiconductor TiO₂ (-4.21 eV vs. vacuum) [16]. From Table 3, it is clear that all the synthesized dyes have less negative LUMO values compared to CB of semiconductor TiO₂ and hence they can accomplish the electron injection and thereby undergo oxidation. This driving force makes the process thermodynamically more favorable.

Frontier Molecular Orbital (FMO) Analysis

To understand the molecular architecture, the electron density distribution of the compounds and to characterize the global chemical parameters, FMO analysis was done by DFT calculations using B3LYP/6-31G (d, p) level software. The geometry optimized structures and electron density distribution of HOMO and LUMO orbitals of the compounds are as shown in Fig. 5.

From Fig. 5, it is observed that electron density distribution in HOMO is concentrated on 2,4-dinitrophenyl moiety and in LUMO concentrated on coumarin moiety in structures 2ad and 2cd. For 2bd, the electron density is moderately distributed between HOMO and LUMO levels. The electron density distribution in HOMO of 2dd is localized on donor coumarin

Table 3 Electrochemical properties of coumarin dyes

Entry	The onset oxidation potential (V)	$E_{\text{HOMO}}^{\text{a}}$ (eV)	$E_{\text{LUMO}}^{\text{a}}$ (eV)	$E_{\text{HOMO}}^{\text{b}}$ (eV)	$E_{\text{LUMO}}^{\text{b}}$ (eV)
2ad	0.3727	-5.47	-3.08	-6.28	-2.80
2bd	0.2873	-5.39	-2.97	-6.20	-2.71
2cd	0.3915	-5.49	-3.08	-6.28	-2.69
2dd	0.1788	-5.28	-3.05	-5.88	-2.57

$$^a E_{\text{HOMO}} = -(E_{\text{onsetox}} + 5.1) \text{ eV and } E_{\text{LUMO}} = E_{\text{HOMO}} + E_{\text{g}}^{\text{opt}}; \text{ where, } E_{\text{onsetox}} \text{ is the onset oxidation potential in V, } E_{\text{g}}^{\text{opt}} \text{ is the optical band gap in eV, and } 5.1 \text{ eV is the assuming electrochemical potential of Fc/Fc}^+ \text{ in vacuum}$$

^b DFT calculations

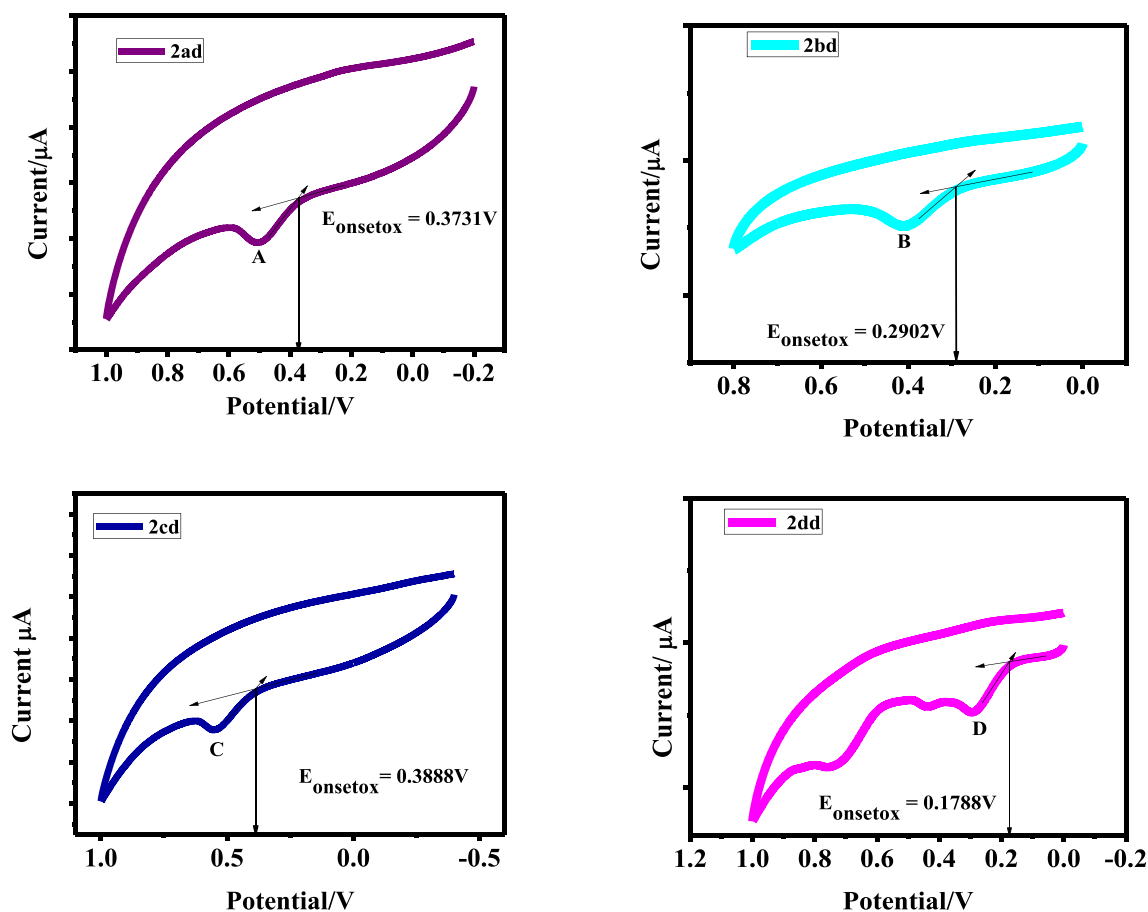


Fig. 4 Cyclic voltammogram of 2ad, 2bd, 2cd and 2dd

moiety through a pi bridge and in LUMO it is shifted towards electron-withdrawing nitro groups of 2,4-DNP and hence it provides good intramolecular charge transfer (ICT) from donor to acceptor leading to push-pull effect [17].

Calculations of Global Chemical Parameters

Using the values of HOMO and LUMO by FMO analysis, the global chemical parameters like ionization energy (I), electron affinity (A), electronegativity (χ), chemical hardness (η) and chemical softness (σ) have been calculated for the understanding of donor-acceptor interactions. These parameters are obtained by Koopmans theorem and are listed in Tables 4 and 5 [18]. According to this theorem, the electron affinity (A) and ionization potential (I) are given by Eq. (2).

$$I = -E_{\text{HOMO}} \text{ and } A = -E_{\text{LUMO}} \quad (2)$$

Ionization energy is defined as the amount of energy required for the removal of an electron from the highest occupied molecular orbital. Electron affinity is the amount of energy released when an electron is added to the lowest unoccupied molecular orbital. These parameters determine the ability

to donate and accept the electrons by the molecules respectively. The electronegativity (χ) is a measure of the intrinsic donor-acceptor character of a molecule and is the algebraic sum of I and A as proposed by Robert S. Mulliken [19] and is given in Eq. (3).

$$\chi = \frac{1}{2}(I + A) \text{ or } \chi = \frac{1}{2}[-E_{\text{HOMO}} + (-E_{\text{LUMO}})] \quad (3)$$

Chemical hardness (η) is the resistance to change the electron distribution or electron density function of a chemical system. It is given by the Eqs. (4) and (5). The lower chemical hardness indicates the small HOMO–LUMO gap and it is desired for better intramolecular charge transfer.

$$\eta = \frac{1}{2}(I - A) \quad (4)$$

$$\eta = E_{\text{g}}/2 \quad (5)$$

Chemical softness (σ) is the reverse of the hardness and is given by Eq. (6).

$$\sigma = (1/\eta) \quad (6)$$

From Tables 4 and 5, the ionization energy is found to be smaller for 2dd compared to others in the series 2ad–2dd. This may be attributed to the presence of strong electron releasing

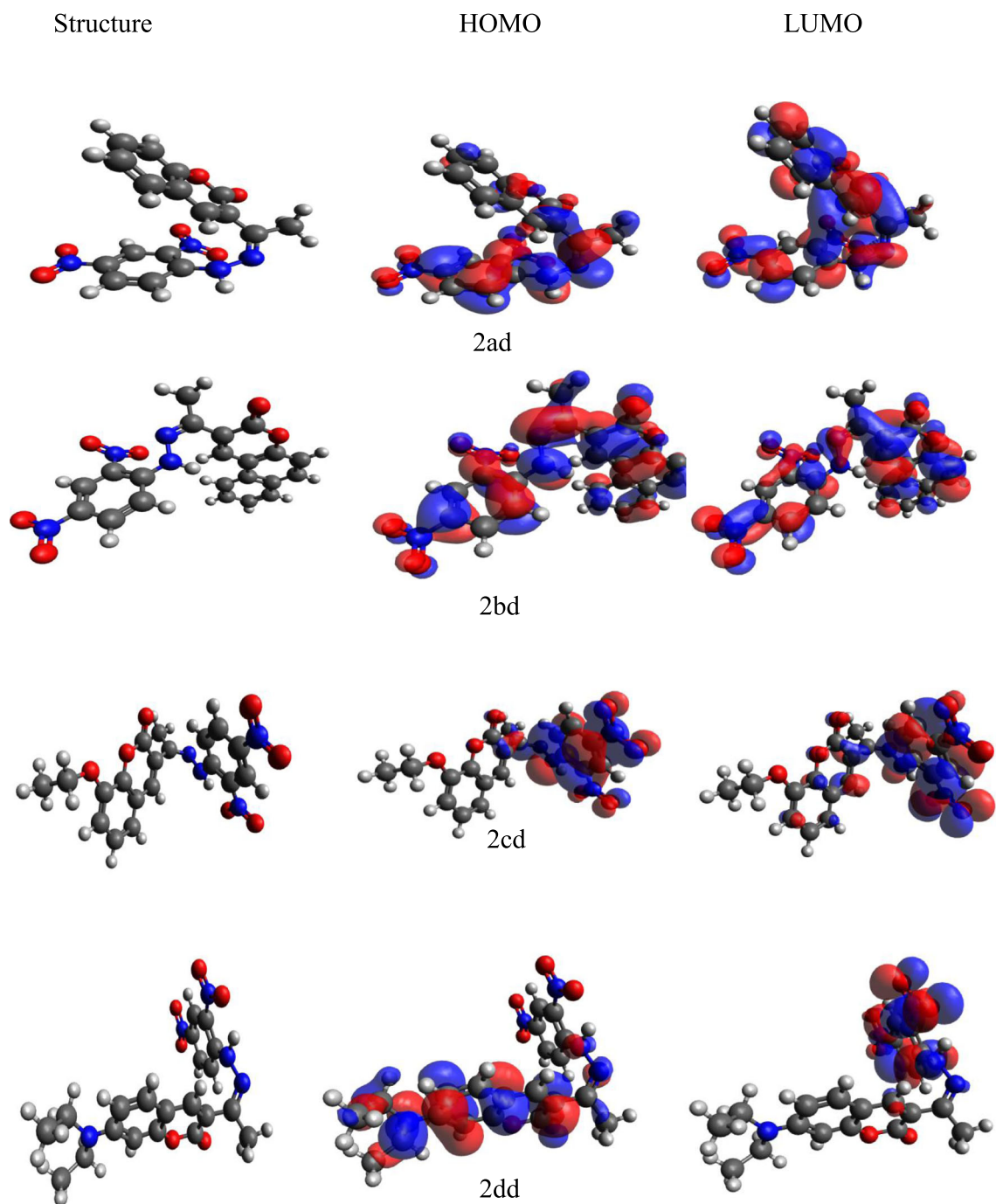


Fig. 5 Molecular architecture and electron density distribution of the compounds calculated by DFT using B3LYP/6-31G (d,p) level software

Table 4 Experimental global chemical parameters of synthesized molecules

Entry	I (eV)	A (eV)	χ (eV)	η (eV)	σ (eV)
2ad	5.47	3.08	4.30	1.20	0.83
2bd	5.39	2.97	4.18	1.21	0.83
2cd	5.49	3.08	4.29	1.21	0.83
2dd	5.28	3.05	4.17	1.12	0.89

Table 5 Theoretical global chemical parameters of synthesized molecules at B3LYP/6-31G (d, p) level software

Entry	I (eV)	A (eV)	χ (eV)	η (eV)	σ (eV)
2ad	6.28	2.80	4.54	1.70	0.59
2bd	6.20	2.71	4.46	1.75	0.57
2cd	6.28	2.69	4.49	1.80	0.56
2dd	5.88	2.57	4.17	1.66	0.60

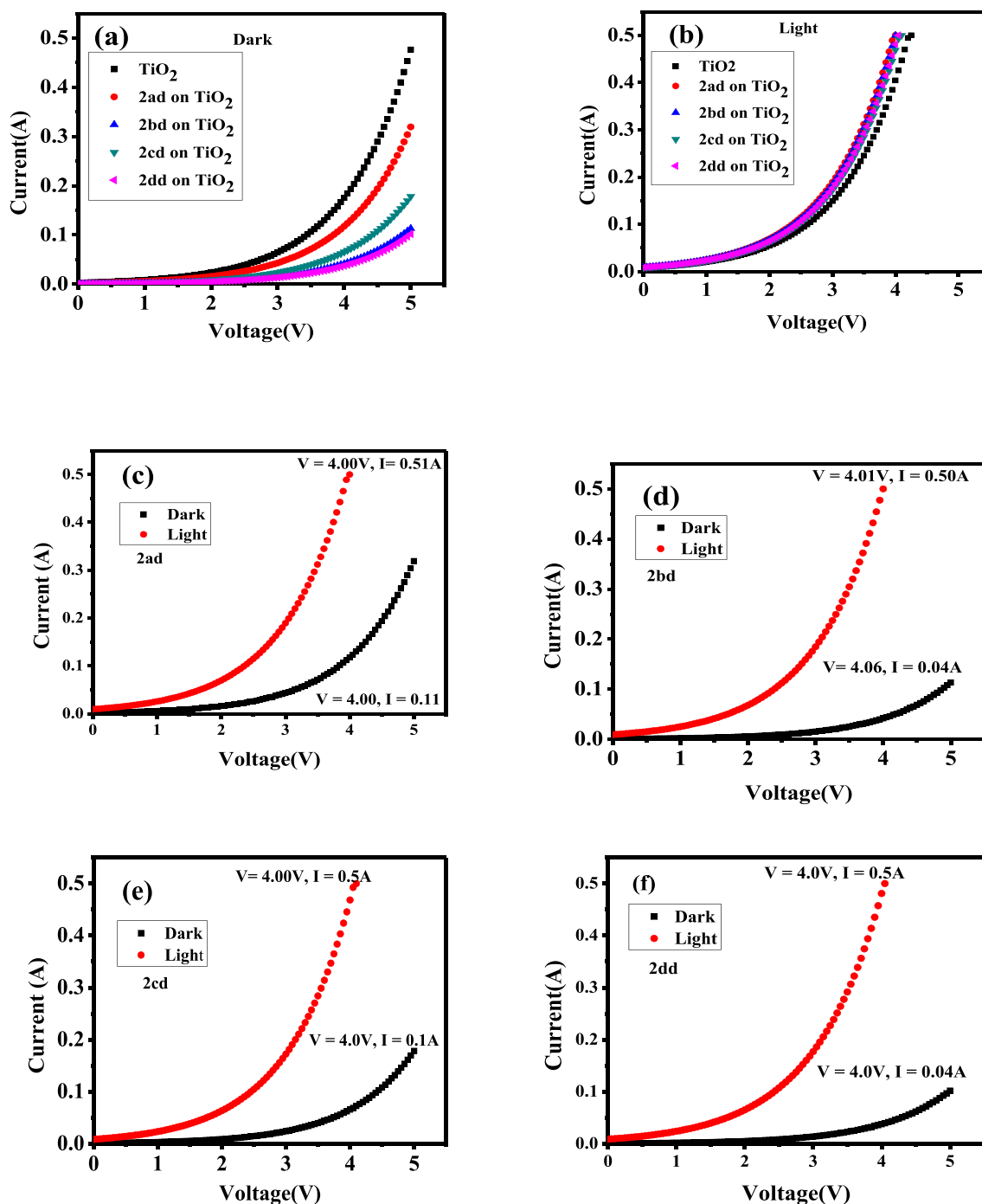


Fig. 6 Current-Voltage (I-V) characteristics of TiO₂ and dye coated TiO₂: **a**-under dark, **b**-under light, **c**, **d**, **e** and **f**: (I-V) characteristics of dyes 2ad, 2bd, 2cd and 2dd on TiO₂ under dark and light condition respectively

group diethyl amine on 7- position of coumarin skeleton. Smaller ionization energy makes this molecule a strong electron donor. The order of decrease in the electron affinity values for series of dyes is as follows 2ad > 2cd > 2bd > 2dd (Table 5). Smaller electronegativity of 2dd is also indicated that 2dd is a strong electron donor compared to others. The electronegativity of 2bd is greater than 2dd but smaller than 2ad and 2cd. This may be explained on the basis of extended

conjugation of coumarin moiety with benzene ring fusion at 5, 6-position. This shows that the electron donation of 2bd is higher than that of 2ad and 2cd. Hard and soft nature of the molecules can be evaluated on the basis of hardness and softness values. From Table 4, 2dd is found to be a softer molecule which is further supported with smaller band gap (Table 2) compared to others in the series. The global chemical parameters computed theoretically using DFT calculation follows

the same trend as that of experimental values except the electron affinity value of 2bd and 2cd. The order of electron affinity values is as follows: 2ad > 2bd > 2cd > 2dd.

Current-Voltage (I-V) Characteristics

The current-voltage response of pure TiO₂ and dyes coated TiO₂ were performed under dark and illumination conditions and shown in Fig. 6.

From Fig. 6a and b, it is clear that the current-voltage response of pure TiO₂ is greater than the dyes coated TiO₂ under dark condition. The lower I-V response of dye coated TiO₂ is attributed to the blocking effect of the dye [20]. The Figs. 6c–f show the photosensitive behaviour of the dyes 2ad, 2bd, 2cd and 2dd on TiO₂ nanoparticles, respectively. It is evident that at the potential of 4.0 V, the current response is higher under light condition (0.5A) compare to dark condition (~0.01A) for all the dyes. This is probably due to an increase in the number and mobility of charge carriers (electron-hole pairs) upon illumination. This enhanced photocurrent of dyes significantly improves the solar cell performance. Hence, these dyes could be considered as good photovoltaic sensitizers.

Conclusion

The coumarin molecules containing electron-withdrawing nitro chromophores have been synthesized using the novel method. The TiO₂ nanoparticles were synthesized by sol-gel method. The optical properties of synthesized dye molecules and dyes coated TiO₂ nanoparticles were studied by measuring the band gap energy. Energy levels of HOMO and LUMO were determined using cyclic voltammetric method and compared with theoretical DFT study. The results show that the energy levels of HOMO and LUMO of the prepared dye molecules were found to be matched with TiO₂ energy levels. I-V characteristics study shown that the prepared dyes could be successfully used for photovoltaic applications.

Acknowledgments Authors are thankful to UGC-SWRO and Department of Collegiate Education-Bangalore for selecting under UGC-FIP scheme. The authors are also thankful to DST (SERB), New Delhi, UGC New Delhi, for providing the instrumental facility.

References

- Chan MMY, Tao CH, Yam VWW (2010) In: Yam V (ed) WOLEDs and organic photovoltaics, green energy and technology. Springer, Heidelberg, p 1. https://doi.org/10.1007/978-3-64214935-1_1
- Fung DDS, Choy WCH (2013) Introduction to organic solar cells. In: Choy W (ed) Organic solar cells green energy and technology. Springer, London, p 1. https://doi.org/10.1007/978-1-4471-4823-4_1
- Hara K, Sayama K, Arakawa H, Ohga Y, Shinpo A, Suga S (2001) A coumarin-derivative dye sensitized nanocrystalline TiO₂ solar cell having a high solar-energy conversion efficiency up to 5.6%. Chem Commun 6:569–570. <https://doi.org/10.1039/B010058G>
- Furniss BS, Hannaford AJ, Smith PWG, Tatchell AR (1989) Vogel's textbook of practical organic chemistry. Wiley, New York
- Razi SS, Ali R, Srivastava P, Misra A (2014) Simple Michael acceptor type coumarin derived turn-on fluorescence probes to detect cyanide in pure water. Tetrahedron Lett 55:2936. <https://doi.org/10.1016/j.tetlet.2014.03.087>
- Allen CFH (1930) The identification of carbonyl compounds by use of 2,4-dinitrophenylhydrazine. J Am Chem Soc 52(7):2955–2959. <https://doi.org/10.1021/ja01370a058>
- Wolfmon ML, Arsenault GP (1960) Preparation of 2,4-dinitrophenylhydrazine derivatives of highly oxygenated carbonyl compounds. J Org Chem 25(2):205–208. <https://doi.org/10.1021/jo01072a014>
- Polizzotti A, Berke JS, Falsgraf E, Johal M (2012) In: Fthenakis V (ed) Third generation photovoltaics. InTech, Croatia, p 111
- Sugino T, Tanaka K (2001) Solvent-free Coumarin synthesis. Chem Lett 30(2):110–111. <https://doi.org/10.1246/cl2001110>
- Vidyasagar CC, Arthoba Naik Y, Venkatesha TG, Manjunatha P (2012) Sol-gel synthesis using glacial acetic acid and optical properties of anatase Cu–TiO₂ nanoparticles. J Nanoeng Nanomanuf 2: 91–98. <https://doi.org/10.1166/jnan.2012.1058>
- Hara K, Kurashige M, Dan-oh Y, Kasada C, Shinpo A, Suga S, Sayama K, Arakawa H (2003) Design of new coumarin dyes having thiophene moieties for highly efficient organic-dye-sensitized solar cells. New J Chem 27:783–785. <https://doi.org/10.1039/B300694H>
- Yathisha RO, Arthoba Nayaka Y, Manjunatha P, Purushothama HT, Vinay MM, Basavarajappa KV (2019) Study on the effect of Zn²⁺ doping on optical and electrical properties of CuO nanoparticles. Physica E: Low-dimensional Systems and Nanostructures 108: 257–268. <https://doi.org/10.1016/j.physe.2018.12.021>
- Hou J, Guo X (2013) Active layer materials for organic solar cells. In: Choy WCH (ed) Organic solar cells. Springer, London. https://doi.org/10.1007/978-1-4471-4823-4_2
- Hara K, Sato T, Katoh R, Furube A, Ohga Y, Shinpo A, Suga S, Sayama K, Sugihara H, Arakawa H (2003) Molecular design of coumarin dyes for efficient dye-sensitized solar cells. J Phys Chem B 107:597–606. <https://doi.org/10.1021/jp026963x>
- Kim B, Ma B, Venkat RD, Liu H, Frechet JMJ (2010) Bodipy-backboned polymers as electron donor in bulk heterojunction solar cells. Chem Commun 46:4148. <https://doi.org/10.1039/B927350F>
- Xu Y, Martin AAS (2000) The absolute energy positions of conduction and valence bands of selected semiconducting minerals. Am Mineral 85:543–556. <https://doi.org/10.2138/am-2000-0416>
- Agrwal S, Pastore M, Marott G, Reddy MA, Chandrashekarm M, Angelis FD (2013) Optical properties and aggregation of phenothiazine-based dye-sensitizers for solar cells applications a combined experimental and computational investigation. J Phys Chem C 117(19):9613–9622. <https://doi.org/10.1021/jp4026305>
- Pearson RG (1997) Chemical hardness. Wiley, Germany, p 38
- Mulliken RS (1934) A new Electroaffinity scale: together with data on valence states and on valence ionization potentials and Electron affinities. J Chem Phys 2:782–793. <https://doi.org/10.1063/1.1749394>
- Stanley A, Matthews D (1995) The dark current at the TiO₂ electrode of a dye-sensitized TiO₂ photovoltaic cell. Aust J Chem 48(7): 1293. <https://doi.org/10.1071/CH9951293>

Publisher's Note Springer Nature remains neutral with regard to jurisdictional claims in published maps and institutional affiliations.